

Efficient polarization beam splitter pixels based on a dielectric metasurface

M. KHORASANINEJAD,^{1*} W. ZHU,¹ K. B. CROZIER,^{1,2,3*}

¹*School of Engineering and Applied Sciences, Harvard University, 33 Oxford Street, Cambridge, MA 02138, USA*

²*Department of Electrical and Electronic Engineering, University of Melbourne, Victoria 3010, Australia.*

³*School of Physics, University of Melbourne, Victoria 3010, Australia*

*Corresponding authors: khosani@seas.harvard.edu and kcrozier@unimelb.edu.au

Received XX Month XXXX; revised XX Month, XXXX; accepted XX Month XXXX; posted XX Month XXXX (Doc. ID XXXXX); published XX Month XXXX

The polarization-dependence of the reflection, refraction and diffraction of electromagnetic waves from materials is measured in applications that extend from small (e.g. ellipsometry of semiconductor chips) to large scales (e.g. remote sensing for planetary science and weather radar). Such applications employ polarimeters that are in turn based on devices with polarization-selective absorption or reflection/refraction properties (e.g. prisms). The latter devices are generally bulky, thereby limiting their integration into compact systems. The former devices are inherently lossy, as they function by absorbing the unwanted polarization. Here, we experimentally demonstrate a conceptually novel method for pixel level polarimetry. Each pixel contains amorphous-silicon (a-Si) nanoridges and deflects incident light in a polarization-dependent manner. As photons are sorted by polarization rather than filtered, the approach permits high efficiency. A high transmission efficiency of 90% and a high extinction ratio of 15 times are demonstrated. © 2014 Optical Society of America

OCIS codes: Polarimetry; (290.5855) Scattering, polarization (160.3918) Metamaterials; (160.4236) Nanomaterials.

<http://dx.doi.org/10.1364/optica.99.099999>

1. INTRODUCTION

Conventional image sensors capture images that record intensity and color but are blind to the polarization state of light. It is known however that polarization-resolved imaging can enhance contrast in hazy/foggy conditions [1], underwater and in turbid media [2-3], and for biological tissues [4-5]. These desirable features have created a strong incentive for the development of imaging modules with integrated polarization filters (one per photodetector pixel) [6]. Such filters generally absorb the unwanted polarization, however, making them inefficient by nature [6-10]. Another type of polarizer is the linearly-polarizing beam splitter [11-14], which is typically built from either a naturally birefringent crystal [13] or from a structure with artificial birefringence [15]. Such polarizers make use of the fact that refraction and reflection at an interface can be highly polarization dependent. They can provide highly efficient polarization splitting, but are unfortunately too large for pixel-level integration.

Recently, dielectric “metasurface” concept has been explored as a means for controlling optical wavefronts using ultra-thin and low-loss elements [16-21]. Here we employ metasurfaces to experimentally realize a polarization beam splitter whose footprint ($5\ \mu\text{m} \times 5\ \mu\text{m}$) is orders of magnitude smaller than those of traditional approaches. This architecture permits integration with image sensors, with one polarization splitter per pixel. We therefore term our device as a pixel-integrated polarization splitter (PIXIP). A PIXIP consists of three amorphous-silicon (a-Si) nanoridges. Each nanoridge acts as a polarization-selective diffractive element, and controls the direction of light propagation based on its polarization. The use of dielectric nanostructures for color filtering has been suggested and demonstrated in several works [22-26]. Nishiwaki *et al* studied silicon nitride ridges for controlling the direction of light propagation [24], but like [22, 23, 25], these were for resolving wavelength rather than polarization. Polarization splitting is achieved for circular polarized light in [16-17]; however, those devices cannot distinguish between linear polarizations and furthermore do not study their pixel level capabilities.

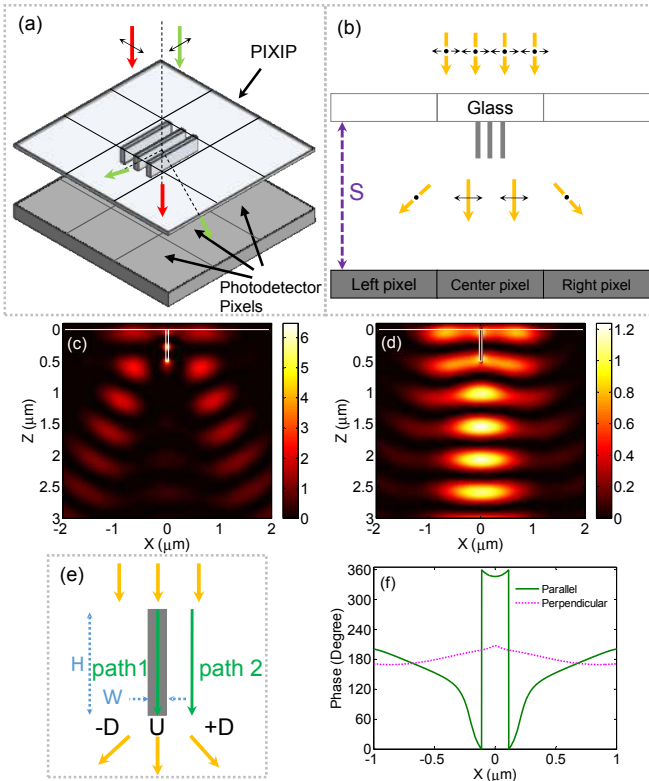


Fig. 1. (a) Perspective view of proposed PIXIP device which consists of three a-Si nanoridges per pixel. For simplicity, only the central pixel's nanoridges are depicted. For polarization perpendicular to the length of nanoridges, impinging light is undeflected (red arrow) and proceeds to the center photodetector pixel. Parallel polarized light, on the other hand, will be re-directed to side photodetector pixels (green arrows). (b) Side view of PIXIP device placed above photodetector pixels, with polarization splitting concept illustrated. (c)-(d) Simulation results showing that single nanoridge acts as a polarization beam splitter. Nanoridge has width $W=60$ nm, height $H=500$ nm and is considered to be infinitely long (in y -direction). (c) Power distribution in x - z plane for case when nanoridge is excited by truncated plane-wave polarized along y -direction. Impinging light strongly interacts with nanoridge and is deflected to sides. (d) Power distribution in x - z plane for case when nanoridge is excited by truncated plane-wave polarized along x -direction. Incident light is largely undeflected. (e) Schematic diagram illustrating mechanism of polarization beam splitting. Nanoridge acts akin to a slab waveguide providing an optical path for incoming light (path 1). There is an alternative optical path (path 2). Phase accumulation is different for these two paths. (f). Simulation results showing that phase accumulation varies with polarization. Phase is recorded at a distance of 50 nm above tip of nanoridge ($z=550$ nm in Fig. 1(c)-(d)). Parallel polarization curve plots phase of y -component of electric field under y -polarized illumination. Perpendicular polarization curve plots phase of x -component of electric field under x -polarized illumination.

The organization of our paper is as follows. We begin by describing the underlying principle of the PIXIP, namely that the high refractive index and elongated shape of an a-Si nanoridge renders its interaction with light highly polarization-dependent. This concept is studied by simulation and experiment. We then show that arrays of a-Si nanoridges function as PIXIP devices at near-infrared wavelengths, a spectral range of importance in applications that include night vision, medical diagnostics, and

environmental monitoring [27-29]. In addition, our device makes use of the low absorption by silicon in the infrared [30].

2. OPERATING PRINCIPLE OF PIXIP DEVICE

Light incident on a nanoridge will in general interact much more strongly with it when it is polarized along the nanoridge length (L) than when it is polarized across its width W (where $W \ll L$) [16, 31]. In this paper, we utilize this polarization-dependence of light-matter interaction along with near-field interference effects to realize our PIXIP devices. Schematic diagrams of how PIXIP devices could be used for imaging polarimetry are shown as Fig. 1(a)-(b). An array of PIXIP devices would be fabricated above the photodetector array of an image sensor (Fig. 1(a)). Each PIXIP would contain three amorphous silicon (a-Si) nanoridges. For convenience, only the central pixel's nanoridges are shown in Fig. 1(a)-(b). The three nanoridges of each PXIP have identical widths W , lengths L (equal to pixel size) and heights H and are located so that they have center-to-center distances of P . The substrate is glass and is spaced from the photodetector array by a distance S . As shown in Fig. 1(b), for polarization perpendicular to the nanoridge length, impinging light is undeflected and proceeds to the "center" photodetector pixel. On the other hand, light with polarization parallel to nanoridge length is re-directed onto the "left" and "right" photodetector pixels. Conventional image sensors achieve color separations using arrays of filters (red, green and blue), with one filter per photodetector and the final image found by de-mosaicking. In an analogous manner, the PIXIP devices steer light in a polarization-dependent manner such that each photodetector pixel only receives a specific polarization. We note here that this method ultimately presents the opportunity for much higher efficiencies than filter-based approaches, as light is sorted onto the appropriate photodetector pixel. In a filter-based approach, on the other hand, light of the unwanted polarization is discarded. In our proposed approach, as the splitting functions of the PIXIP devices are known beforehand, polarization-resolved images can be obtained from the photodetector outputs.

In order to understand the principle of operation, we first theoretically study the simple case of a single nanoridge on a glass substrate. The nanoridge has width $W=60$ nm, height $H=500$ nm and is infinitely long (i.e. simulations are two dimensional). The illumination beam is a truncated plane-wave ($2.5 \mu\text{m}$ wide) and has a free space wavelength of $\lambda=1 \mu\text{m}$. Its polarization is either parallel (Fig. 1(c)) or perpendicular (Fig. 1(d)) to the nanoridge length. As expected for parallel polarization, light strongly interacts with the nanoridge, giving rise to a distinct scattering pattern (Fig. 1(c)). However for the perpendicular polarization, scattering significantly diminishes and the beam is instead slightly focused (Fig. 1(d)). Further insight into the splitting mechanism is gained by considering the nanoridge as a slab waveguide (Fig. 1(e)). A portion of the impinging light is coupled to its guided mode (path 1), while the rest either propagates adjacent to the nanoridge (path 2) or is scattered away (not shown here). Interference between light traveling along these two paths depends of course on the phase difference between them. If the phase difference is small, then the outgoing light is undeflected ("U" in Fig. 1(e)). On the other hand, if the phase difference is an odd multiple of π , there will be a strong destructive interference between the paths, with the transmission in the forward direction suppressed, and the outgoing light instead being deflected into directions " $\mp D$ " (Fig. 1(e)). To further explore this, we plot the phase of the electric field at a distance of 50 nm beyond the top of the nanoridge in Fig. 1(f). For the case of the incident light being polarized parallel to the

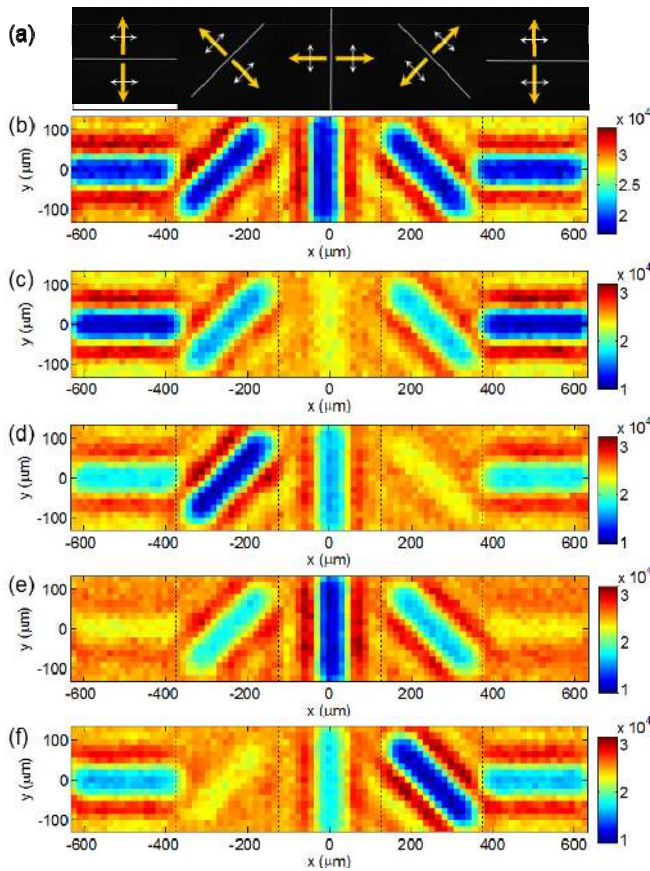


Fig. 2. (a) Top-view SEM of fabricated structure, scale bar: 5 μm . White arrows have been added to show the polarization component that is deflected by each nanoridge. Yellow arrows have been added to show deflection direction. Nanoridges have lengths $L=5\ \mu\text{m}$, widths $W=60\ \text{nm}$ and heights $H=500\ \text{nm}$ and are spaced by 5 μm (center-to-center). (b)-(f) Experiments: images of structure under illumination from IR-LED with (b) random, (c) zero degree, (d) 45 degree, (e) 90 degree and (f) 135 degree polarization.

nanoridge length, it is the y -component of the electric field phase that is plotted. For the case of the incident light being polarized perpendicular to the nanoridge length, it is the x -component of the electric field phase that is plotted. It can be seen that, for the parallel polarization, the difference in the phase between the field of path 1 (i.e. at nanoridge center $x \approx 0\ \mu\text{m}$) and that of the field of path 2 (i.e. at $x \approx \pm 0.5\ \mu\text{m}$) is close to ~ 180 degrees (resulting in deflected beam, Fig. 1(c)). For the perpendicular polarization, this phase difference is far smaller, resulting in the beam not being deflected, but instead loosely focused (Fig. 1(d)). We also calculate the effective index of the waveguide using the beam propagation method, yielding effective indices of 2.11 and 1.02 for parallel and perpendicular polarization, respectively. Using these indices, the phase difference between waveguide and air over 500 nm propagation are 199.8 and 3.6 degrees for parallel and perpendicular polarization, respectively. This is reasonably consistent with the FDTD results.

3. RESULTS

A. Experimental demonstration of polarization-dependent scattering by nanoridges

To demonstrate the polarization-dependent beam splitting capability of PIXIP devices, we begin by considering single

nanoridges. The starting substrate is a glass wafer that is cleaned in acetone, with sonication. Plasma-enhanced chemical vapor deposition (PECVD) is then used to deposit a-Si to a thickness of 500 nm. Phosphine is introduced during the a-Si deposition to dope it, thereby enhancing its conductivity and preventing charge accumulation from degrading the resolution of the electron beam lithography (EBL) step that occurs later. The wafer is next spin coated with poly(methyl methacrylate) (PMMA, 950K A2) at a speed of 4000 rpm and baked on a hotplate at 180 $^{\circ}\text{C}$ for 5 minutes. Electron beam exposure is performed using an Elionix ELS-F125 system operating at 125 kV. The resist is then developed in a mixture of methyl isobutyl ketone and isopropyl alcohol (MIBK:IPA is 1:3) at room temperature for 30 s, dipped in IPA for 30 s, and then blown dry by nitrogen. Aluminum is then deposited by electron beam evaporation at the rate of 2 $\text{\AA}/\text{s}$ to a thickness of 20 nm. Lift-off is carried out by soaking the sample in a solvent stripper (Remover PG from Microchem). Inductively coupled plasma-reactive ion etching (ICP-RIE) is performed to etch the nanoridges [32]. The passivation layer generated during the etching process is removed by placing the device in an oxygen plasma (power: 150 W) for 5 minutes. The device is completed by removing the aluminum mask by soaking the sample in developer (MF319 from Shipley) for 5 minutes. Optical measurements are then performed. Our test structure consists of a-Si nanoridges, each with length $L=5\ \mu\text{m}$, width $W=60\ \text{nm}$ and height $H=500\ \text{nm}$. A scanning electron microscope (SEM) of the structure is shown as Fig. 2(a); more SEMs of the structure are provided in Fig. S1 of Supplementary Material (SM). It can be seen that the unit cell consist of four pixels, each containing a nanoridge. The nanoridges successively rotate by 45 $^{\circ}$. In Fig. 2(a), we also graphically indicate the fact that each nanoridge deflects light polarized along its length. To demonstrate this experimentally, measurements are performed using a homebuilt optical microscope (Figure S2 of SM). The measurement set-up consists of a LED (M940L3 from Thorlabs) with a center wavelength of 940 nm and spectral width (full-width at half maximum, FWHM) of 37 nm. The output beam is collected with a condenser and then passes through a linear polarizer. The linear polarizer is adjusted to generate the desired input polarization. The light transmitted by the PIXIP device is collected by a microscope objective lens (magnification 50 \times) and, in combination with the subsequent tube lens (focal length of 15 mm), an image is formed on a camera. We begin by considering the case where there is no linear polarizer in the beam path. The light impinging upon the nanoridge sample is therefore randomly polarized. Half of the incident light power impinging on each nanoridge is polarized parallel to its length, with the other half polarized perpendicular to it. The images of the nanoridges formed on the camera (Fig. 2(b)) each therefore have the same characteristic pattern (with the appropriate rotation). The simulation of Fig. 1(c) predicts that, for the parallel polarization, the intensity distribution at the end of the nanoridge should show a minimum above the nanoridge, with maxima adjacent to the nanoridge (parallel to it). Similarly, that of Fig. 1 (d) predicts that, for the perpendicular polarization, the intensity distribution at the end of the nanoridge should be largely flat. We next add a linear polarizer between the condenser and the sample. We align the polarizer so that light polarized along the x -direction is transmitted. For this polarization, the horizontal nanoridge (i.e. aligned along the x -direction) is expected to scatter light, and thus show an intensity distribution with a minimum above the nanoridge and maxima adjacent (and parallel) to it. Fig. 2(c) confirms that this does indeed occur experimentally. It can also be seen that the vertical nanoridge (i.e. aligned along the y -direction) generates negligible scattering resulting in a flat light distribution.

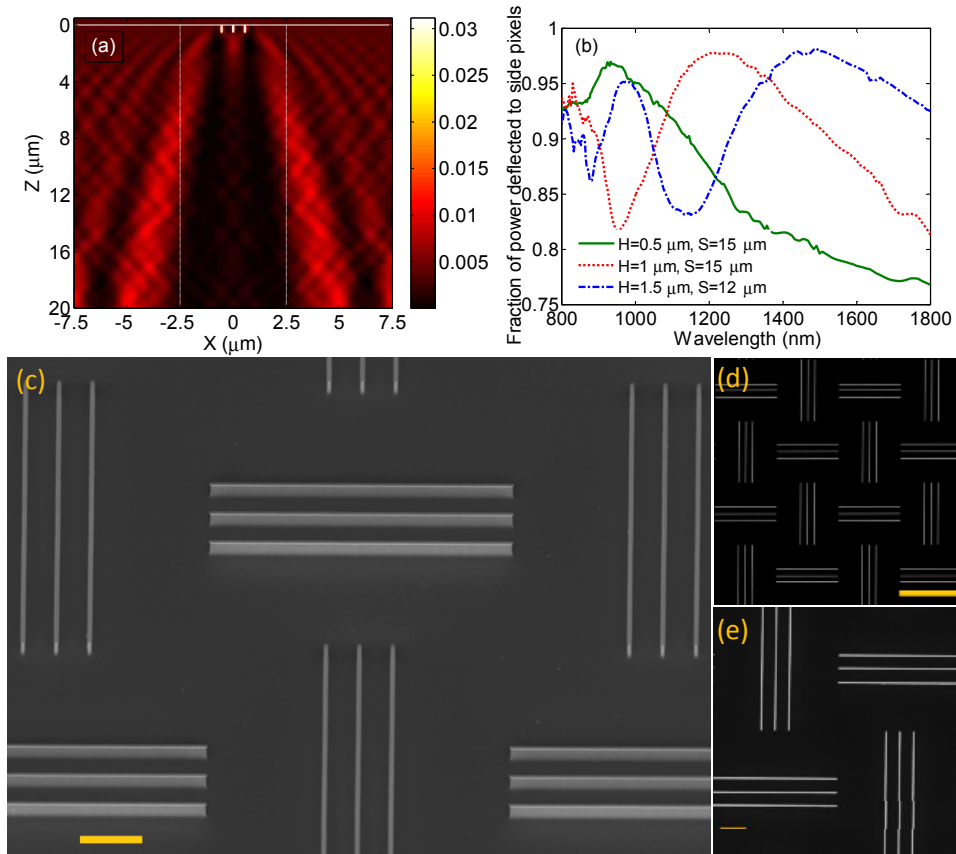


Fig. 3. (a) Simulated power flow for light polarized parallel to length of nanoridges (y -direction). Wavelength of operation is $\lambda=950 \text{ nm}$. There are three nanoridges with widths $W=50 \text{ nm}$, heights $H=500 \text{ nm}$, center-to-center distance $P=550 \text{ nm}$, and lengths $L=5 \mu\text{m}$. After $z=14 \mu\text{m}$ majority of power presents in side pixels region. Boundaries of pixels are highlighted by dashed lines. For this simulation, the total transmission, reflection and absorption are 94.5%, 5% and 0.5 % respectively. (b) Fraction of transmitted power that is deflected to side pixels versus wavelength for three different designs. Designs are optimized for center wavelengths close to 1000 nm, 1200 nm and 1500 nm. By deviating from design wavelength, phase difference will no longer takes the value π ; therefore, we shift from “destructive interference condition”, and the proportion of input light power that is split (deflected) is reduced. For all simulations, there are three nanoridges with widths $W=50 \text{ nm}$, center-to-center distance $P=550 \text{ nm}$ and lengths $L=5 \mu\text{m}$. Heights of nanoridges and distance from substrate where power is recorded are noted in figure’s caption. (c)-(e) SEMs of fabricated PIXIP device. (c) Tilted-view SEM of PIXIP device, scale bar is 1 μm . (d) Top-view SEM of PIXIP device, scale bar is 5 μm . (e) Top-view SEM depicting one unit cell of PIXIP device, scale bar is 1 μm .

The nanoridges aligned at angles of 45° and 135° (from the x -direction) scatter the component of the incident (x -polarized) illumination that is polarized along their long axes. These nanoridges are not of course expected to scatter the x -polarized illumination as strongly as the horizontal nanoridge. The experimental results verify this (Fig. 2(c)). We next align the polarizer to be at 45° from the x -axis, i.e. polarization is along the length of the second nanoridge from the left. It can be seen from Fig. 2(d) that this nanoridge (45° orientation) scatters strongly, that the horizontal and vertical nanoridges scatter (but not as strongly) and that the scattering from the 135° orientation nanoridge (second from right) is the weakest. Experiments are also performed with the linear polarizer set to 90° and 135° , and we observe the same trends (Fig. 2(e)-(f)). These experimental results demonstrate the polarization-dependent scattering properties of the nanoridges. By modifying the orientation of the nanoridge, therefore, the direction that light is steered into can be adjusted. In the next section, we show that this mechanism enables efficient polarizers with high extinction ratios.

B. Experimental demonstration of PIXIP devices

We now employ the polarization-dependent light scattering properties of nanoridges to realize our proposed PIXIP devices. The appropriate number of nanoridges in each pixel will of course depend on the pixel size. A single nanoridge has a limited effective interaction area in which it can sort photons based on their polarization. To increase the effective interaction area, one can increase the number of nanoridges. One might initially expect that increasing the number of nanoridges will result in larger reflection and in excitation of higher order diffraction side lobes, both of which contribute to loss. Our simulations however show that using three nanoridges, one can extend the interaction area to the size of a pixel, here $5 \mu\text{m} \times 5 \mu\text{m}$, while simultaneously maintaining low loss. Keeping this in mind, we vary their widths, heights and spacing. For each configuration, we simulate the fields produced for the cases of illumination parallel and perpendicular to the ridges. Because in the intended device the nanoridges are far longer ($L=5 \mu\text{m}$) than they are wide, we employ two-dimensional (2D) simulations. We monitor the power flow at different distances from the nanoridges, allowing us to determine the

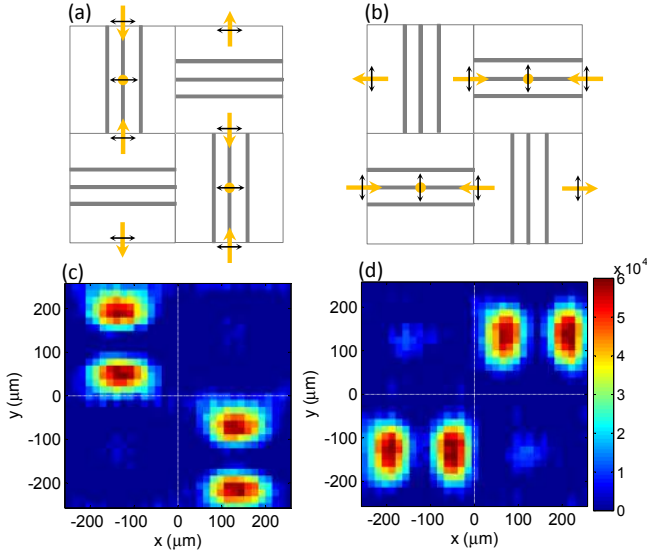


Fig. 4. (a)-(b) Top view of one unit cell of PIXIP showing how nanoridges steer impinging light with (a) horizontal polarization (along x -direction) and (b) vertical polarization (along y -direction). (c)-(d) Experimental results: intensity distributions over one unit cell of PIXIP device, with imaging plane at $15 \mu\text{m}$ from PIXIP device, for input polarizations along (c) x - and (d) y -directions.

signals that would be recorded by the photodetectors of the image sensor in the proposed configuration of Fig. 1(a). In this design procedure, the aims are as follows. When the polarization is perpendicular to the nanoridges, the fraction of the incident power that would be transmitted to the center photodetector should be as high as possible. Similarly, when the polarization is parallel to the nanoridges, the fraction of the incident power that is deflected to the side (left and right) photodetectors should similarly be as high as possible. The optimal design is that producing the greatest contrast between parallel and perpendicular polarizations, as well as high throughput. In Fig. 3(a), we show simulation result of PIXIP, where the center pixel contains three nanoridges with widths $W=50$ nm, heights $H=500$ nm, lengths $L=5 \mu\text{m}$ and spacing $P=550$ nm. We assume periodic boundary conditions at the x -axis and y -axis (for three dimensional simulations) boundaries and perfectly matched layers (PML) at the z -axis boundaries. The mesh size is 5 nm for both the x - and z -directions. The refractive indices of the a-Si layer are measured by ellipsometry over the wavelength range of interest, and those values are used in the simulations. We note that the real and imaginary part of refractive index at $\lambda=950$ nm are measured to be $n=3.64$ and $k=0.006$, respectively which are very close to values of $n=3.68$, $k=0.002$ reported in [33]. The structure is illuminated with a plane-wave at wavelength $\lambda=950$ nm with polarization parallel to the length of nanoridges. It can be seen from Fig. 3(a) that the structure redirects the light to the left and right sides in an effective manner. The center pixel region is depleted of light beyond a distance of $14 \mu\text{m}$, with the majority of power flux propagating to the side pixels which contribute to left and right pixel at the image sensor. To quantify the spectral behavior of the PIXIP structure, the amount of power deflected to the side pixels is calculated for parallel polarized light. These results are plotted as a function of illumination wavelength in Fig. 3(b) for three different designs with center wavelengths close to $\lambda=1000$ nm, 1200 nm, and 1500 nm. As much as 95% of transmitted power is deflected to the side pixels. In addition, it can be seen that splitting occurs over a wide spectral range, especially for designs having long center wavelengths. So far we have shown

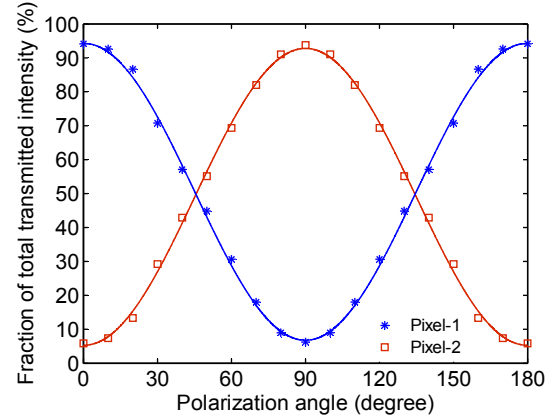


Fig. 5. Fraction of total intensity received by pixel-1 and pixel-2 at distance of $S=15 \mu\text{m}$ from device versus polarization angle.

symmetric beam splitting in which beam is symmetrically deflected in a two-way manner (to the left and right). For some applications one might interested in asymmetric deflection (e.g. single-sided deflection) rather than symmetric deflection. This capability is demonstrated in the SM using an array of eleven nanoridges whose widths successively increase across the array (Figure S3 of SM).

The PIXIP devices are fabricated using the same top-down approach described earlier for the single nanoridge structures. SEMs are shown in Fig. 3(c)-(e). Each pixel has a size of $5 \mu\text{m} \times 5 \mu\text{m}$ and contains three nanoridges with widths $W=50$ nm, lengths $L=5 \mu\text{m}$, heights $H=500$ nm and spacing $P=550$ nm. The unit cell comprises four pixels for which the constituent nanoridges are rotated by 90° but are otherwise identical. Nanoridges are arranged in such a way that each photodetector pixel receives light impinging upon its corresponding PIXIP pixel, less that directed from it by its nanoridges, plus that directed onto it from adjacent PIXIP pixels. In this scheme, the splitting function of each nanoridge pattern is known a priori which make it possible to generate polarization resolved images from the photodetector outputs via a matrix operation. Figures 4(a)-(b) illustrate the splitting behavior schematically for horizontal (parallel to x -axis) and vertical (parallel to y -axis) polarizations, with the deflection and polarization directions shown as yellow and black arrows, respectively. As shown, incident light will be deflected to neighboring pixels when its polarization is aligned along the nanoridge length. On the other hand, incident light will be undeflected when its polarization is perpendicular to the nanoridge length. Our experimental results (Figure 4(c)-(d)) confirm that this function is achieved. The results are obtained as follows. As before (Fig. 2), the device is illuminated with polarized infrared light ($\lambda=940$ nm). A microscope objective (N.A.0.55) and tube lens are used to form an image of the device on the CCD camera. The device is then moved away from the microscope lens by a distance of $15 \mu\text{m}$. The image recorded by the CCD camera then corresponds to the intensity distribution that would be recorded by a photodetector array placed at this distance from the device. Figures 4(c)-(d) show the intensity distributions recorded by the CCD for one PIXIP unit cell, for polarization along the x - (horizontal) and y -directions (vertical), respectively. For x -polarized illumination, the majority of the output power (94%) is directed to the top-left and bottom-right pixels, with fraction of power being directed to the top-right and bottom-left pixels being very small (6%). For the y -polarized illumination, the power is directed to the top-right and bottom-left pixels, with the power to

the top-left and bottom-right pixels again being small (Fig. 4(d)). An extinction ratio of 15 (94%/6%) is achieved in this polarization splitting scheme. More importantly the output power is 90% of input power. This value is measured by dividing the power integrated over one unit cell ($10\mu\text{m}\times 10\mu\text{m}$) by the power integrated over a region with the same area on the glass substrate adjacent to the PIXIP structure where there are no nanoridges. In addition, this measured output power is very close to the value of 92 % predicted by 3D simulation of the actual device. The intensity distributions of a larger region of the device (10×10 pixels, i.e. 5×5 unit cells) are shown in Fig. S4 of SM. It can be seen that the polarization-splitting behavior is consistent across the array. It is interesting to note that the area of the nanoridges (projected onto the xy -plane) is only 3% of the total area. That the filling fraction is small means that the writing time of the EBL step is relatively short. For example the writing time for a very large PIXIP device ($2.4\text{ mm}\times 2.4\text{ mm}$) is only ~ 2 hours, which is comparatively short for EBL, given the overall extent of the device.

In order to quantify the splitting performance of the PIXIP device, we measure the power received by two representative pixels as a function of polarization angle. These are termed pixel-1 and pixel-2, and correspond to the top-left and top-right pixels of Fig. 4(c), respectively. For each polarization angle, we record the experimentally-measured intensities integrated over pixels 1 and 2. The results are plotted as Fig. 5, and show that the transmitted power gradually switches from pixel-1 to pixel-2 as polarization angle changes from zero (horizontal polarization) to 90 degrees (vertical polarization). Intensity distributions measured for one unit cell of the PIXIP device over this range of polarization angles are shown as Fig. S5 of SM. The power switches back to pixel-1 when the polarization angle is varied from 90 to 180 degrees.

4. CONCLUSION

In summary, we present a new concept for polarization-splitting using a-Si nanoridges. This polarization dependent photon-sorting capability provides a new mechanism to encode polarization at the pixel level with a device architecture that is extremely compact and, being based on a dielectric, has very low loss. Our approach has a number of attractive features, including high efficiency and extinction ratio, simplicity and straightforward fabrication, scalability from the visible-to-infrared frequencies, and reproducibility on large scales. When integrated with an image sensor, the proposed PIXIP devices could enable high efficiency polarization-resolved imaging with promising applications in microscopy, security, night vision, astronomical observation, and free-space communication networks. These polarizer elements could potentially also play crucial roles in other applications, such as polarization information encryption [34-35] and nonlinear optics [36]. In addition, there is the obvious potential for extending the concept to more spectral bands, especially into the mid/far-infrared where a-Si maintains its low loss. For extension into the visible wavelength range, gallium phosphide could be used. Its refractive index is high (similar to silicon in the infrared), but it has low loss.

FUNDING INFORMATION

National Science Foundation (NSF) (ECCS-1307561 and ECCS-1201687) Australian Research Council (Discovery Project, DP150103736), and the Victorian Endowment for Science, Knowledge and Innovation (VESKI)

ACKNOWLEDGMENTS

Fabrication work was carried out in the Harvard Center for Nanoscale Systems, which is supported by the NSF. We thank Dr. Ethan Schonbrun from the Rowland Institute at Harvard for lending us a light emitting diode.

REFERENCES

1. S. Shwartz, E. Namer, Y. Schechner, "Blind Haze Separation," *Proc. IEEE Comp. Vision and Pat. Recog.*, **2**, 1984–1991, (2006).
2. T. Treibitz, Y. Schechner, "Active polarization descattering," *IEEE Trans. Pattern Anal. Mach. Intell.*, **31**, 385–399, (2009).
3. J. S. Tyo, M. P. Rowe, E. N. Pugh Jr., N. Engheta, "Target detection in optically scatter media by polarization-difference imaging," *Appl. Opt.*, **35**, 1855–1870, (1996).
4. W. Groner, J.W. Winkelman, A.G. Harri, C. Ince, G.J. Bouma, K. Messmer, R.G. Nadeau, "Orthogonal polarization spectral imaging: A new method for study of the microcirculation," *Nature Med.*, **5**, 1209–1213, (1999).
5. R.S. Gurjar, V. Backman, L. T. Perelman, I. Georgakoudi, K. Badizadegan, I. Itzkan, R. R. Dasari, M. S. Feld, "Imaging human epithelial properties with polarized light scattering spectroscopy," *Nat. Med.*, **7**, 1245–1248, (2001).
6. V. Gruev, R. Perkins, T. York, "CCD polarization imaging sensor with aluminum nanowire optical filters," *Opt. Express*, **18**, 19087–19094, (2010).
7. G. R. Bird, M. Parrish Jr., "The Wire Grid as a Near-Infrared Polarizer," *J. Opt. Soc. Am.* **50**, 886, (1960).
8. E. Laux, C. Genet, T. Skauli, T. W. Ebbesen, "Plasmonic photon sorters for spectral and polarimetric imaging," *Nature Photon.*, **2**, 161–164, (2008).
9. J. Elliott, I. I. Smolyaninov, N. I. Zheludev, A. V. Zayats, "Polarization control of optical transmission of a periodic array of elliptical nanoholes in a metal film," *Opt. Lett.*, **29**, 1414–1416, (2004).
10. T. Ellenbogen, K. Seo, K. B. Crozier, "Chromatic plasmonic polarizers for active visible color filtering and polarimetry," *Nano Lett.*, **12**, 1026–1031, (2012).
11. W. Nicol, "On a method of so far increasing the divergence of the two rays in calcareous-spar, that only one image may be seen at a time," *Edinb. New Philos. J.*, **6**, 83–84 (1829).
12. P. Glan, "Über einen polarisator," *Rep. Exptl-Physik*, **16**, 570–573 (1880).
13. M. Bass, "Handbook of Optics," McGraw-Hill, (2001).
14. D. Goldstein, "Polarized Light," 2nd edn Marcel Dekker, (2003).
15. Y. Shen, D. Ye, I. Celanovic, S. G. Johnson, J. D. Joannopoulos, M. Soljačić, "Optical Broadband Angular Selectivity," *Science*, **343**, 1499, (2014).
16. M. Khorasaninejad, K. B. Crozier, "Silicon nanofin grating as a miniature chirality-distinguishing beam-splitter," *Nat. Commun.*, **5**, 5386, (2014).
17. D. Lin, P. Fan, E. Hasman, and M. L. Brongersma, "Dielectric gradient metasurface optical elements," *Science* **345**, 298 (2014).
18. M. Decker, I. Staude, M. Falkner, J. Dominguez, D. N. Neshev, I. Brener, T. Pertsch, and Y. S. Kivshar "High-Efficiency Dielectric Huygens' Surfaces," *Adv. Opt. Mater.*, 201400584 (2015).
19. Y. Yang, W. Wang, P. Moitra, I. I. Kravchenko, D. P. Briggs, and Jason Valentine. "Dielectric meta-reflectarray for broadband linear polarization conversion and optical vortex generation," *Nano Lett.*, **14**, 1394–1399, (2014).
20. I. Staude and *et al.* "Tailoring Directional Scattering through Magnetic and Electric Resonances in Subwavelength Silicon Nanodisks," *ACS Nano* **7**, 7824 (2013).
21. C. Wu and *et al.* "Spectrally Selective Chiral Silicon Metasurfaces Based on Infrared Fano Resonances," *Nat. Comm.* **5**, 3892 (2014).
22. M. Khorasaninejad, N. Abedzadeh, J. Walla, S. Patchett, and S. S. Saini, "Color matrix refractive index sensors using coupled vertical silicon nanowire arrays," *Nano Lett.* **12**, 4228–4234 (2012).
23. K. Seo, M. Wober, P. Steinvurzel, E. Schonbrun, Y. P. Dan, T. Ellenbogen, K. B. Crozier, "Multicolored vertical silicon nanowires," *Nano Lett.*, **11**, 1851–1586, (2011).

24. S. Nishiwaki, T. Nakamura, M. Hiramoto, T. Fujii, M. Suzuki, "Efficient colour splitters for high-pixel-density image sensors," *Nat. Photonics.*, **7**, 248–254 (2013).
25. M. Khorasaninejad, S. Patchett, J. Sun J, N. O, and S. S. Saini, "Diameter dependence of polarization resolved reflectance from vertical silicon nanowire arrays: evidence of tunable absorption," *J. Appl. Phys.* **114** 024304 (2013).
26. J. Walia, N. Dhindsa, M. Khorasaninejad, and Saini S S, "Color generation and refractive index sensing using diffraction from 2D silicon nanowire arrays" *Small* **10** 144–51 (2014).
27. M. Phillips, N. Ho, "Infrared hyperspectral imaging using a broadly tunable external cavity quantum cascade laser and microbolometer focal plane array," *Opt. Express*, **16**, 1836, (2008).
28. M.C. Martin, C. Dabat-Blondeau, M. Unger, J. Sedlmair, D. Y. Parkinson, H. A. Bechtel, B. Illman, J. M. Castro, M. Keiluweit, D. Buschke, B. Ogle, M. J. Nasse, C. J. Hirschmugl, "3D spectral imaging with synchrotron Fourier transform infrared spectro-microtomography," *Nat. Methods*, **10**, 861–864, (2013).
29. A. Rogalski, "Infrared detectors: an overview," *Infrared Phys. Technol.*, **43**, 187–210 (2002).
30. E. D. Palik, "Handbook of Optical Constants of Solids," Ed. Academic: Orlando, FL, (1985).
31. M. Khorasaninejad, N. Abedzadeh, J. Sun, J. N. Hilfiker, S. S. Saini, "Polarization resolved reflection from ordered vertical silicon nanowire arrays," *Opt. Lett.*, **37**, 2961–2963, (2012).
32. M. Khorasaninejad, J. Walia, and S. S. Saini, "Enhanced first-order Raman scattering from arrays of vertical silicon nanowires", *Nanotechnology* **23**, 275706 (2012)
33. D. T. Pierce and W. E. Spicer "Electronic Structure of Amorphous Si from Photoemission and Optical Studies" *Phys. Rev. B* **5**, 3017, (1972).
Refractive indices from this reference are also reported in:
<http://refractiveindex.info/?shelf=main&book=Si&page=Pierce>
34. P. Refregier, B. Javidi, "Optical image encryption based on input plane and Fourier plane random encoding," *Opt. Lett.*, **20**, 767–769, (1995).
35. A. Lamas-Linares, J. C. Howell, D. Bouwmeester, "Stimulated emission of polarization-entangled photons," *Nature*, **412**, 887–890 (2001).
36. Y. R. Shen, "Principles of Nonlinear Optics," Wiley, New York, (1984).